Monitoring the Spatio-temporal Evolution of a Reconnection X-line in Space

Z. Wang[1] , H. S. Fu[1] , A. Vaivads[2], J. L. Burch[3] , Y. Yu[1], and J. B. Cao[1]
[1] School of Space and Environment, Beihang University, Beijing, People's Republic of China; huishanf@gmail.com
[2] KTH Royal Institute of Technology, Stockholm, Sweden
[3] Southwest Research Institute, San Antonio, TX, USA

Abstract

Inherently, magnetic reconnection—the process responsible for stellar flares and magnetospheric substorms—is very dynamic in space, owing to magnetic fluctuations and unsteady inflows. However, this process was always explained as a static picture in spacecraft measurements, neglecting the temporal evolution. This picture is not correct. Here we provide the first dynamic picture of magnetic reconnection in space, by monitoring the spatio-temporal evolution of a reconnection X-line at the magnetopause. Surprisingly, we find that the angle of a reconnection X-line can change from $44°\!\!.8$ to $24°\!\!.9$ during tens of milliseconds, which is significantly smaller than the characteristic timescale of the reconnection process ($t = d_i/V_A \sim 410$ ms). Meanwhile, the spacecraft moves from the inflow region to the outflow region (spatial evolution). This result demonstrates that the magnetic reconnection in space can develop rapidly during tens of milliseconds, and thus that the concept of dynamic reconnection should be invoked instead of a static diagram.

1. Introduction

To date, magnetic reconnection—the process explosively converting magnetic energy into particle energy (Priest & Forbes 2000; Yamada et al. 2010; Fu et al. 2017, 2019c) and simultaneously changing magnetic topology to an X-line shape —has been reported in the solar corona (Shibata et al. 1995), interplanetary medium (Phan et al. 2006), planetary magnetopause (Burch et al. 2016b) and magnetotail (Angelopoulos et al. 2008; Torbert et al. 2018), and laboratory experiments (Ji et al. 1998; Egedal et al. 2007). In all these regions, plasmas are turbulent due to the large Lundquist number (Ji & Daughton 2011; Cao et al. 2013; Fu et al. 2014; Higashimori et al. 2013; Liu et al. 2019b), and thus the reconnection processes there are very dynamic. Figure 1 illustrates this dynamic reconnection process at the Earth's magnetopause, which is attributed either to (1) the time-varying solar wind speed that results in an unsteady inflow velocity during reconnection (Fu et al. 2013a, 2013b), (2) the turbulent magnetosheath that results in oscillation of the reconnecting magnetic fields (Retinó et al. 2007), (3) the plasmaspheric plume that affects the plasma density and Alfvén velocity in the reconnection region (Walsh et al. 2014), or (4) the self-driven turbulence by the 3D reconnection process itself (Daughton et al. 2011).

Although magnetic reconnection in space is dynamic, the in situ measurement of this process was always explained as a static picture. raditionally, scientists have drawn a static diagram of the reconnection region and then inferred spacecraft trajectories on top of this diagram (see, for example, the insert in Figure 1) according to the spacecraft measurements of plasmas and magnetic fields (Mozer et al. 2002; Wei et al. 2007; Angelopoulos et al. 2008; Paschmann et al. 2013; Burch et al. 2016b; Cao et al. 2017; Torbert et al. 2018; Hesse & Cassak 2020) or reconstructed the reconnection region in a stationary state (Hasegawa et al. 2017). Such approaches can resolve complex spacecraft trajectories (for example, the back-and-forth motion of spacecraft relative to the reconnection X-line), but the overall property of magnetic reconnection derived from these approaches is static. In other words, these approaches can reveal the spatial evolution of magnetic reconnection but neglect the temporal evolution, which over-simplifies the reconnection process in space.

Monitoring the spatio-temporal evolution of the reconnection X-line is a key step for uncovering the reconnection process in space. The First-Order Taylor Expansion (FOTE) technique (Fu et al. 2015), developed particularly for the Magnetospheric Multiscale (MMS) mission (Burch et al. 2016a), enables us to solve this problem: at a specific time, the FOTE technique not only can reconstruct the topology of a reconnection X-line but also can resolve the spacecraft positions relative to this X-line (Fu et al. 2015); by considering a series of MMS measurements in the reconnection region, the topology of a reconnection X-line can be continuously reconstructed (temporal evolution) and the spacecraft positions relative to the X-line can be continuously resolved (spatial evolution). As a result, the spatio-temporal evolution of an reconnection X-line can be monitored. So far, this technique has been applied to the MMS mission (Chen et al. 2018, 2019a, 2019b; Liu et al. 2018, 2019a; Fu et al. 2019a, 2019b; Wang et al. 2019, 2020). By utilizing this technique, here we provide the first dynamic picture of magnetic reconnection in space.

2. Overview of Event

The event that we consider was detected by MMS on 2015 October 16, at about 13:07 UT, when it was located near the Earth's magnetopause at $(8.3, 8.5, -0.7)$ R_E (GSE coordinates). In this event, the four MMS spacecraft, forming a regular tetrahedron 14 km in size, crossed the magnetopause boundary layer from south to north (see the black arrow in Figure 1). They measured very similar magnetic fields (Figures 2(a)–(b)) and plasma flow velocities (Figure 2(c)), as their separation was quite small (compared to the local ion inertial length $d_i = c/\omega_{pi} \approx 78$ km). Similar magnetic fields and flow
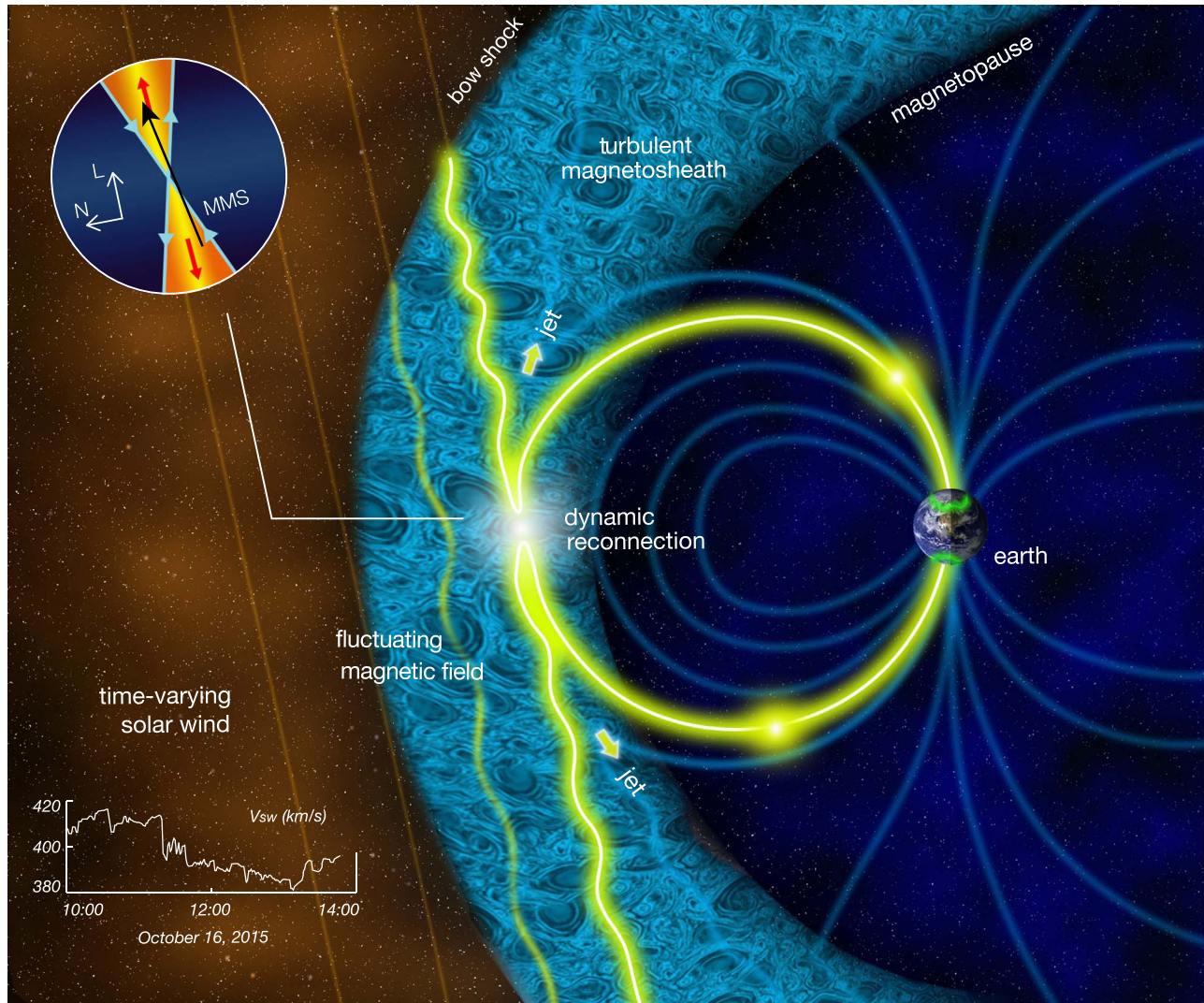
Figure 1. A concept of dynamic magnetic reconnection at Earth's magnetopause, shown in the noon-midnight plane. The red area on the left, the green area in the middle, and the dark area on the right denote the interplanetary space, magnetosheath, and the Earth's magnetosphere, respectively. The shiny lines, linking the magnetosphere with the interplanetary space, mark an ongoing reconnection process at the magnetopause. This reconnection process is intrinsically dynamic, because (1) the inflow velocity of magnetic reconnection is unsteady—induced by the time-varying solar wind speed in the interplanetary space, (2) the reconnecting magnetic field lines are oscillating—induced by the magnetic fluctuation in the turbulent magnetosheath, and (3) the plasma density and Alfvén velocity in the reconnection region can change—induced by the plasmaspheric plume in the magnetosphere. Correspondingly, the dynamic reconnection produces pulse auroras in the dayside ionosphere. The insert is a static picture, showing the Magnetospheric Multiscale (MMS) trajectory across the reconnection region (in LMN coordinates). The fluctuating line shows the solar wind speed during magnetic reconnection on 2015 October 16.

velocities measured by the four spacecraft indicate that the magnetic field changed linearly around the MMS tetrahedron.

In this event, MMS observed a background flow along the southward direction ($V_{iL} \approx -200$ km s^{-1}, see the dashed line in Figure 2(c)) and a flow-reversal signature superposed on this background flow (Figure 2(c)). Near the flow-reversal point (13:07:02 UT), MMS measured an abrupt change of magnetic field from $B_L \approx +20$ nT to $B_L \approx -10$ nT (Figure 2(a)), a significant increase of electron velocity up to $V_{eM} \approx 1600$ km s^{-1} (Figure 2(d)), and a clear violation of the electron frozen-in condition ($E + V_e \times B \neq 0$, see Figure 2(e)). All these features, including the ion-flow reversal (Figure 2(c)), "out-of-plane" electron jet (Figure 2(d)), and electron demagnetization (Figure 2(e)), indicate that MMS was crossing an active electron diffusion region (EDR).

Indeed, this event has been identified as an EDR hosting magnetic reconnection (Burch et al. 2016b). However, to explain this event, scientists utilized a static diagram of simulation and then inferred the spacecraft trajectory on top of this diagram (Burch et al. 2016b) or alternatively reconstructed the EDR as a static picture (Hasegawa et al. 2017). These methods oversimplify the reconnection process, because they give a constant reconnection figure. Actually, in the framework of static reconnection, scientists struggled to fully understand this event, so they suspected the happening of "time-dependent" processes (Hasegawa et al. 2017). We examine the upstream condition in this event and find that the solar wind speed was fluctuating between 380 and 420 km s^{-1} (see the velocity profile in Figure 1) and the magnetic field near the reconnection site was oscillating from 13:07:00 to 13:07:02 UT (see Figures 2(a)–(b)). Both of them indicate that the magnetic reconnection in this event is unsteady and therefore it should be explained as a dynamic reconnection process.
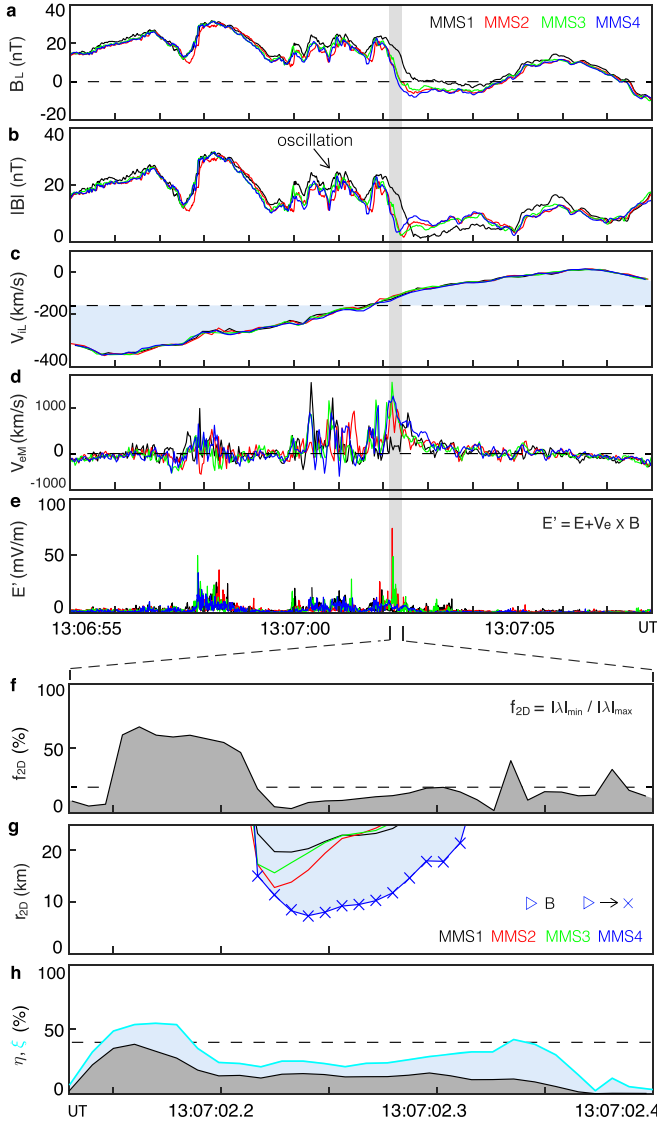
Figure 2. Evidence of dynamic magnetic reconnection at Earth's magnetopause, measured by MMS on 2015 October 16. Data are presented in LMN coordinates. Relative to Geocentric Solar Ecliptic (GSE) coordinates, $L = (0.37, -0.12, 0.92)$, $M = (0.57, -0.76, -0.32)$, and $N = (0.74, 0.64, -0.21)$. (a) The magnetic field B_L component. (b) The magnetic field strength. (c) The ion flow velocity V_{iL} component. (d) The electron flow velocity V_{eM} component. (e) The magnitude of electric fields in the electron-motion frame, for examining the frozen-in condition of electrons. (f–h) Analyses of magnetic nulls during 13:07:02.1–13:07:02.4 UT using the FOTE technique. Specifically shown are (f) the dimensionality factor, with $f_{2D} < 20\%$ denoting a 2-D structure and $f_{2D} > 50\%$ denoting a 3-D structure; (g) the distance from magnetic null to each spacecraft projected in the reconnection plane (termed 2-D distance); and (h) the two parameters, η and ξ, for quantifying the quality of the FOTE results. In (a–e), the black, red, green, and blue lines describe the measurements of MMS 1–4; whereas in (g), they denote the distance from magnetic null to MMS, 1–4 respectively. In (g), the symbol "▷" represents B null, while the symbol "X" indicates that such null can degenerate to 2-D X-null (to distinguish with the B-type nulls that cannot be seemed as 2-D structures/X-nulls, the B-type nulls with $f_{2D} < 0.2$ are marked with blue "X" symbol).

3. Identification of Magnetic Nulls

During crossing of the EDR, MMS sometimes measured magnetic fields close to zero (Figure 2(b)), indicating the potential existence of magnetic nulls in this event (note that the so-called "guide field," if it exists, may slightly affect the null-spacecraft distance but does not affect the identification of
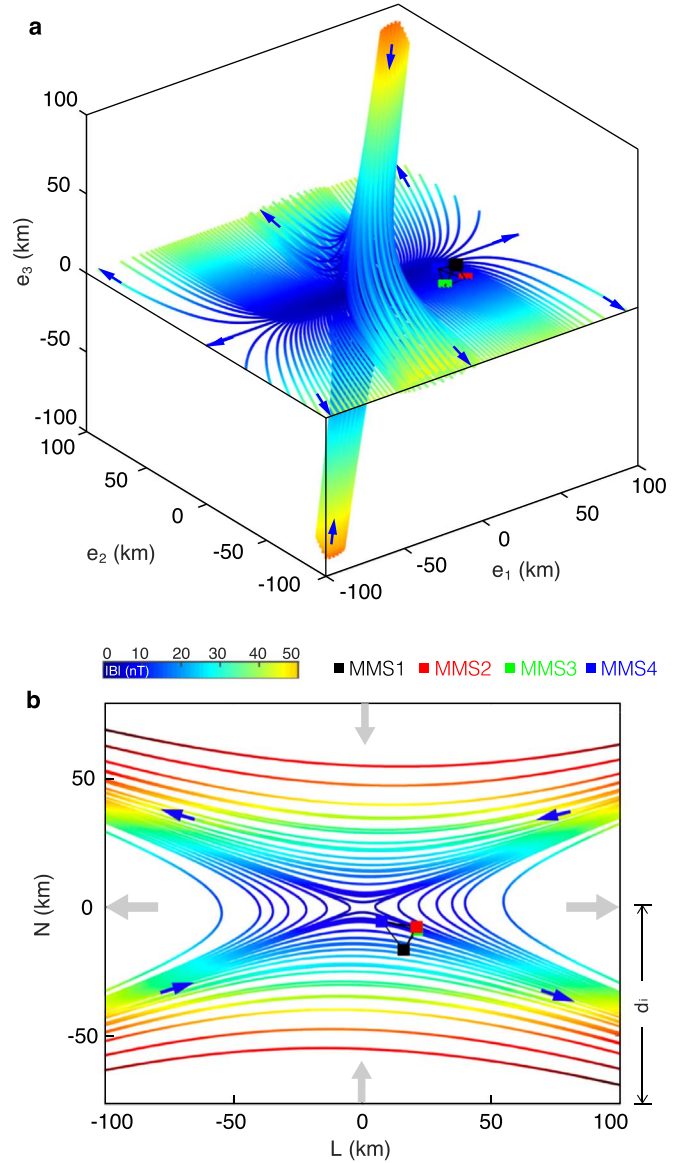

Figure 3. Magnetic field topology around MMS at 13:07:02.25 UT, reconstructed using the FOTE technique. At that time, the Jacobian matrix δB derived from four-spacecraft measurements of magnetic fields has three eigenvectors, $v_1 = (0.77, -0.20, 0.60)$, $v_2 = (0.14, -0.18, 0.97)$, $v_3 = (-0.55, 0.83, -0.01)$, and correspondingly three eigenvalues, $\lambda_1 = 0.06$, $\lambda_2 = -0.36$, $\lambda_3 = 0.41$. Using these eigenvectors, we can establish a new coordinate system $e_1 \ e_2 \ e_3$, in which one axis is along the spine of the null. Relative to GSE coordinates, $e_1 = (-0.55, 0.83, -0.01)$, $e_2 = (0, 0, -1)$, and $e_3 = (-0.83, -0.55, 0.02)$. By tracing and inverse-tracing a few points around the magnetic null, we can obtain the null topology. (a) Magnetic field topology shown in eigenvector coordinates. (b) Magnetic field topology shown in LMN coordinates. The color scale denotes magnetic field strength, while the blue arrows indicate magnetic field direction. The black, red, green, and blue squares represent MMS 1–4, respectively. As the dimensionality factor is very small in this event, the null exhibits a 2D appearance.

magnetic-null properties; see Fu et al. 2016; Fu et al. 2019a). In particular, we focus on the interval 13:07:02.1–13:07:02.4 UT, when the flow reversal and electron demagnetization are the most clear (see the vertical gray shade in Figure 2). Using the FOTE technique, we search for magnetic nulls and analyze null properties during this period. Such properties, derived from the Jacobian matrix δB measured by the four spacecraft, include the dimensionality of the structure, null types, distance from magnetic null to each spacecraft, and the angle between the two
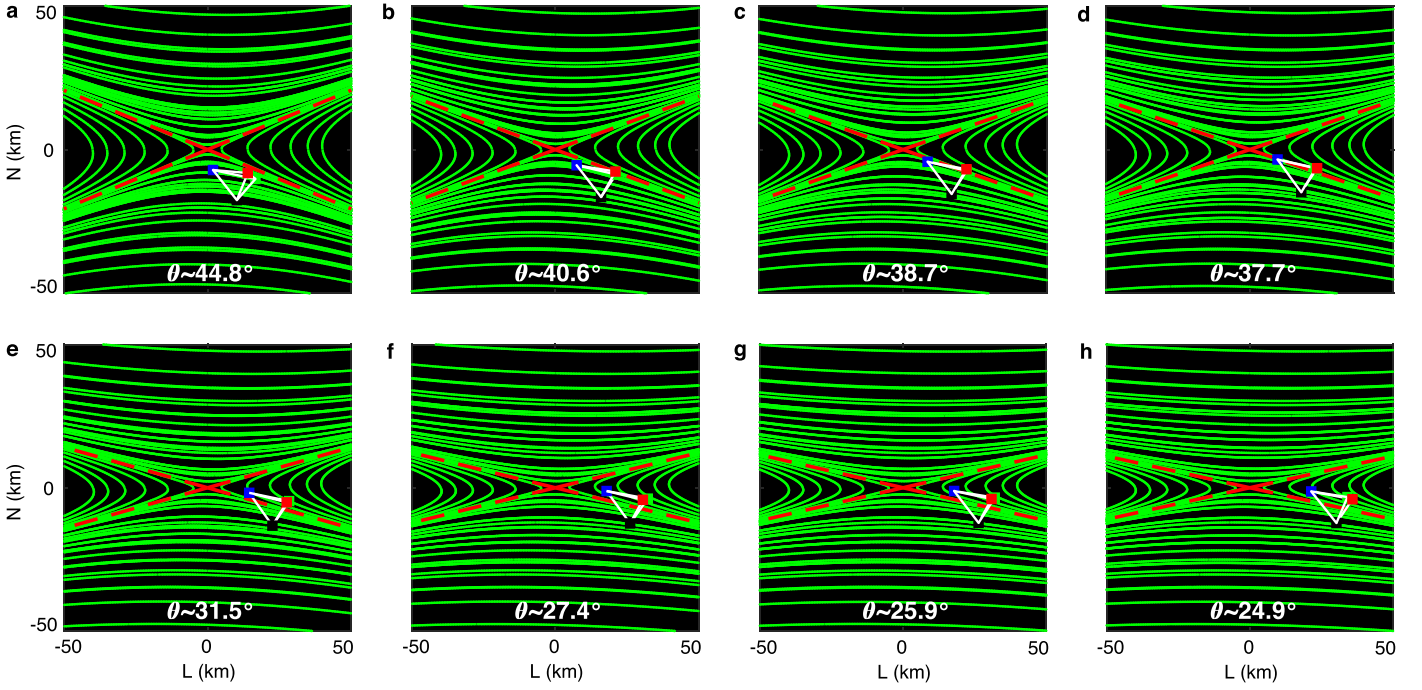
Figure 4. Monitoring the spatio-temporal evolution of magnetic reconnection X-line. The interval is from 13:07:02.24 to 13:07:02.31 UT, with a step-length of 0.01 s. All the magnetic field topologies are shown in LMN coordinates. At each time, the black, red, green, and blue squares represent MMS 1–4, respectively. The center of such spacecraft tetrahedron moves from (10, 10 km) at 13:07:02.24 UT to (35, 2 km) at 13:07:02.31 UT. The angles between the two separatrix lines are (a) $\theta = 44^\circ\!.8$, (b) $\theta = 40^\circ\!.6$, (c) $\theta = 38^\circ\!.7$, (d) $\theta = 37^\circ\!.7$, (e) $\theta = 31^\circ\!.5$, (f) $\theta = 27^\circ\!.4$, (g) $\theta = 25^\circ\!.9$, (h) $\theta = 24^\circ\!.9$. To focus on the topology change, we do not show the magnetic strength around the X-null.

separatrix lines. Specifically, the Jacobian matrix $\delta\boldsymbol{B}$ has three eigenvectors, $\boldsymbol{v}_1$, $\boldsymbol{v}_2$, $\boldsymbol{v}_3$, and three eigenvalues, λ_1, λ_2, λ_3. The dimensionality of the structure is defined as $f_{2D} \equiv |\lambda|_{min}/|\lambda|_{max}$, with $f_{2D} < 0.2$ indicating a 2D structure and $f_{2D} > 0.5$ indicating a 3D structure. The null types are identified using the relationship of the three eigenvalues (e.g., when all of them are real, the null is of radial-type, which includes A-type null (one positive eigenvalue) and B-type null (one negative eigenvalue). They can, however, degenerate into 2D structures as X-null if one of the eigenvalues is zero ($f_{2D} < 0.2$; see more details in Fu et al. 2015), the distance from magnetic null to each spacecraft is resolved from $\boldsymbol{r}_i = \boldsymbol{B}_i/\delta\boldsymbol{B}$, and the angle between the two separatrix lines is defined as the angle between the two eigenvectors that are related to the two large eigenvalues.

To guarantee that the null positions are accurately resolved, we require the null-spacecraft distance (r_i) to be less than 78 km (1 d_i; see the quantitative validation in Fu et al. 2015). Also, to guarantee that the null properties are accurately identified, we define two parameters ($\eta \equiv |\nabla \cdot \boldsymbol{B}|/|\nabla \times \boldsymbol{B}|$ and $\xi \equiv |(\lambda_1 + \lambda_2 + \lambda_3)|/|\lambda|_{max}$) and require them to be smaller than 0.4 (see the quantitative validation in Fu et al. 2015). If the magnetic null is a 2D structure (for example, X-null), we only consider the null-spacecraft distance in the reconnection plane (r_{2D}), because the distance in the out-of-plane direction is meaningless and can cause large uncertainties.

The analysis results are shown in Figures 2(f)–(h). As can be seen, during 13:07:02.22–13:07:02.32 UT, B-type nulls were found by MMS (Figure 2(g)). Because the values of η and ξ are small ($\eta < 0.4$, $\xi < 0.4$; see Figure 2(h)) and the null-spacecraft distance is short ($r_{2D} < 25$ km, see Figure 2(g)), we are confident that these results are accurate. Owing to the small dimensionality factor ($f_{2D} < 0.2$, see Figure 2(f)), the B-null

(3D) in this event can degenerate to X-null (2D). Gradually, the 2D null-spacecraft distance decreases first and then increases (see Figure 2(g)), meaning that MMS was passing the X-null.

4. Topology Reconstruction

We trace and inverse-trace magnetic field lines to obtain the null topology at 13:07:02.25 UT. We show such topology in both the eigenvector coordinates (Figure 3(a)) and LMN coordinates (Figure 3(b)). We find that in eigenvector coordinates the magnetic topology has a "radial" feature, with the magnetic field diverging in the fan plane and converging along the spine (see Figure 3(a)), consistent with the theoretical model of B-null (Lau & Finn 1990; Pontin 2011). In LMN coordinates, the magnetic topology exhibits an "X-line" shape in the LN plane (see Figure 3(b)), with an angle of $40^\circ\!.6$ between the two separatrix lines. Such an "X-line" shape confirms that the 3D B-null in this event can degenerate to a 2D X-null one. Clearly, MMS4 is closest to the X point in the LN plane (Figure 3(b)), with the minimum null-spacecraft distance of $r_{2D} \approx 6$ km (about three electron inertial lengths); MMS1 is farthest from the X-point ($r_{2D} \approx 20$ km; see Figure 3(b)), which may explain why the out-of-plane electron jet was observed by MMS 2–4 but missed by MMS1 during the current-sheet crossing (see the vertical gray shade in Figure 2(d)). The X-line has no asymmetry feature (Figure 3(b)), which is reasonable because (1) the density gradient across the current sheet is small (from 7 to 9 cm^{-3}) in this event, and (2) the reconstruction domain (<100 km) is not large enough to include the asymmetry, which is prominent on a large scale but not on a small scale (Cassak & Shay 2007).

5. Spatio-temporal Evolution of Reconnection X-line

Using the same technique, we continuously reconstruct the magnetic topology around MMS in LMN coordinates from 13:07:02.24 to 13:07:02.31 UT and show them in Figure 4. Because the reconstruction is within a scale of 50 km (0.6 d_i), we are confident that these results are very reliable (Fu et al. 2015). They exhibit both the spatial and temporal evolutions of magnetic reconnection. During spatial evolution, MMS4 moves from the inflow region (Figure 4(a)) to the outflow region (Figure 4(h)); during temporal evolution, the angle between two separatrix-lines gradually decreases from $\theta = 44°.8$ (Figure 4(a)) to $\theta = 24°.9$ (Figure 4(h)). Compared with the characteristic timescale of the reconnection process ($t = d_i/V_A \sim 410$ ms, where d_i is the local ion inertia length and V_A is the Alfvén speed), the spatio-temporal evolution, which has a timescale of tens of milliseconds, is very rapid.

6. Discussion

These results, which show the spatio-temporal evolution of magnetic reconnection in space for the first time, demonstrate that the reconnection process can develop rapidly during tens of milliseconds. To understand it, the conventional concept—assuming a static diagram and inferring spacecraft trajectory on top of this diagram—is not enough. Instead, the concept of dynamic magnetic reconnection should be invoked.

ORCID iDs

Z. Wang ⓘ https://orcid.org/0000-0002-1720-964X
H. S. Fu ⓘ https://orcid.org/0000-0002-4701-7219
J. L. Burch ⓘ https://orcid.org/0000-0003-0452-8403

References

Angelopoulos, V., McFadden, J. P., Larson, D., et al. 2008, Sci, 321, 931
Burch, J. L., Moore, T. E., & Giles, B. L. 2016a, SSRv, 199, 5
Burch, J. L., Torbert, R. B., Phan, T. D., et al. 2016b, Sci, 352, 1189
Cao, D., Fu, H. S., Cao, J. B., et al. 2017, GeoRL, 44, 3954
Cao, J. B., Ma, Y. D., Parks, G., et al. 2013, JGRA, A118, 313
Cassak, P. A., & Shay, M. A. 2007, PhPl, 14, 102114
Chen, X. H., Fu, H. S., Liu, C. M., et al. 2018, ApJ, 852, 17
Chen, Z. Z., Fu, H. S., Liu, C. M., et al. 2019a, GeoRL, 46, 5698
Chen, Z. Z., Fu, H. S., Wang, T. Y., et al. 2019b, SciCh, 62, 144
Daughton, W., Roytershteyn, V., Karimabadi, H., et al. 2011, NatPh, 7, 539
Egedal, J., Fox, W., Katz, N., et al. 2007, PhRvL, 98, 015003
Fu, H. S., Cao, J. B., Cao, D., et al. 2019a, GeoRL, 46, 48
Fu, H. S., Cao, J. B., Cully, C. M., et al. 2014, JGRA, 119, 9089
Fu, H. S., Cao, J. B., Khotyaintsev, Yu. V., et al. 2013a, GeoRL, 40, 6023
Fu, H. S., Cao, J. B., Vaivads, A., et al. 2016, JGRA, 121, 1263
Fu, H. S., Khotyaintsev, Y. V., Vaivads, A., et al. 2013b, NatPh, 9, 426
Fu, H. S., Peng, F. Z., Liu, C. M., et al. 2019b, GeoRL, 46, 5645
Fu, H. S., Vaivads, A., Khotyaintsev, Y. V., et al. 2015, JGRA, 120, 3758
Fu, H. S., Vaivads, A., Khotyaintsev, Y. V., et al. 2017, GeoRL, 44, 37
Fu, H. S., Xu, Y., Vaivads, A., et al. 2019c, ApJL, 870, L22
Hasegawa, H., Sonnerup, B. U. O., Denton, R. E., et al. 2017, GeoRL, 44, 4566
Hesse, M., & Cassak, P. 2020, JGRA, 125, e2018JA025935
Higashimori, K., Yokoi, N., & Hoshino, M. 2013, PhRvL, 110, 255001
Ji, H., & Daughton, W. 2011, PhPl, 18, 111207
Ji, H., Yamada, M., Hsu, S., & Kulsrud, R. 1998, PhRvL, 30, 3256
Lau, Y. T., & Finn, J. M. 1990, APJ, 350, 672
Liu, C. M., Chen, Z. Z., Wang, Z., et al. 2019a, ApJ, 871, 209
Liu, C. M., Fu, H. S., Cao, D., et al. 2018, ApJ, 860, 128
Liu, Y. Y., Fu, H. S., & Liu, C. M. 2019b, ApJL, 877, L16
Mozer, F. S., Bale, S. D., & Phan, T. D. 2002, PhRvL, 89, 015002
Paschmann, G., Oieroset, M., & Phan, T. 2013, SSRv, 178, 385
Phan, T. D., Gosling, J. T., Davis, M. S., et al. 2006, Natur, 439, 175
Pontin, D. I. 2011, AdSpR, 47, 1508
Priest, E. R., & Forbes, T. G. 2000, Magnetic Reconnection: MHD Theory and Applications (Cambridge: Cambridge Univ. Press)
Retinó, A., Sundkvist, D., Vaivads, A., et al. 2007, NatPh, 3, 235
Shibata, K., Masuda, S., Hara, H., et al. 1995, ApJL, 451, L83
Torbert, R. B., Burch, J. L., Phan, T. D., et al. 2018, Sci, 362, 1392
Walsh, B. M., Foster, J. C., Erickson, P. J., & Sibeck, D. G. 2014, Sci, 343, 1122
Wang, Z., Fu, H. S., Liu, C. M., et al. 2019, GeoRL, 46, 1195
Wang, Z., Fu, H. S., Olshevsky, V., et al. 2020, ApJS, 249, 10
Wei, X. H., Cao, J. B., Zhou, G. C., et al. 2007, JGRA, 112, A10225
Yamada, M., Kulsrud, R., & Ji, H. 2010, RvMP, 82, 603